DOI: 10.13009/EUCASS2017-122

Simple body force model for Dielectric Barrier Discharge plasma actuator

Yacine Babou[⋆†]*, Edgar Nieto Martin*[⋆] *and Pablo Fajardo Peña*[⋆]
[⋆]*Departamento de Bioingeniería Ingeniera Aeroespacial, Universidad Carlos III de Madrid*
Avenida de la Universidad 30, 28911, Leganes, Madrid, Spain
edgarnietomartin@gmail.com · pfajardo@ing.uc3m.es
[†]ybabou@ing.uc3m.es

Abstract

The present contribution addresses a simplified expression of the distribution of the Electro Hydrodynamic (EHD) force generated by a single Radio frequency (RF) Dielectric Barrier Discharge (DBD) plasma actuator. By combining judiciously different models previously reported, an upgraded EHD body force model has been elaborated in order to get an expression depending exclusively on the plasma actuator design and operating settings which can be effortlessly implemented as a source term in commercial flow solvers. The performance of the model is assessed through a series of flow computation addressing various arrangements involving multiple actuators. Namely the case of in-series actuator configuration and the case of flipped actuator configuration. Comparisons with flow measurements reported in the literature have shown the relevancy of the adopted modeling approach as well as room for model improvements.

1. Introduction

Airflow actuation by means of Electro Hydrodynamic (EHD) force exploit electrical discharge (or plasma) to transfer momentum to the neutral species through collisions with ions, produced and accelerated by the application of external electric field (or electromagnetic field). During the past decade, surface Dielectric Barrier Discharge (DBD) plasmas have demonstrated substantial potential to generate effective EHD force of interest for current aeronautical applications encompassing boundary layer control[1–3] as well as noise mitigation .[4] A generic DBD plasma actuator consists of two linear parallel electrodes strip (∼1-10 mm width), separated by a layer of dielectric material (∼0.1-10 mm thickness) and arranged in an asymmetric fashion: one electrode displayed on the dielectric surface and exposed to air and the other embedded within the material. Setting the embedded electrode to the ground and applying to the exposed electrode a voltage above few kilo Volts, alternating at Radio Frequency (RF) of order of ∼1-100 kHz, a surface DBD discharge is sustained at atmospheric pressure that injects momentum to the air at the vicinity resulting in flow actuation. Although an alternating voltage is employed, the averaged momentum is directed from the exposed to the embedded electrode as a consequence of the electron accumulation on the dielectric layer during half cycle of voltage alternation.[5] Hence, as a resulting mean effect, the air is pushed downstream generating of thrust of about ∼0.01-0.1 N/m and reaching a velocity of ∼1-10 m/s. Leaning on the practical simplicity of the RF-DBD actuator implementation and operation, various concepts have flourished[6,7] and have been assessed for large set of designs (e.g. electrodes shape: non-linear, non-flat) and powering settings features (e.g. voltage waveforms: sinus, square triangle, sawtooth[8]).

Despite countless attempts, yet the performances of a single actuator remain insufficient for aeronautical applications, where it is a matter of dealing with flow of about 80 m/s speed and higher. To overcome such limitation, approaches based on multi-actuators have been elaborated since the beginning in order to enhance, cumulate or combine the momentum production.[9] In that perspective, the reliable prediction of the RF-DBD actuator effect on a realistic flow stands as a decisive step to develop, assess and optimize multi-actuators concepts, prior to their implementation and testing in wind tunnels. As a rule, the prediction of the EHD force produced by a single RF-DBD plasma actuator requires to solve for highly non-linear system of equations stemming to the strong coupling between the weakly ionized flow (described with Navier-Stokes equation) and the self-consistent electric field (governed by Poisson's equation). The multiple-scale processes such as convection, diffusion, charge accumulation and reaction/ionization mechanisms make the continuity equations of the plasma dynamics stiff.[10] Although such type of computations, addressing the multiple-scale mechanisms, are necessary to understand the underlying mechanism participating to the production of

DOI: 10.13009/EUCASS2017-122

EHD force, it is not a tractable approach for engineering applications aimed to assess the actual potential of multi-actuators system implemented on sophisticated geometries (3D wing, blade trailing edge, landing gear, ...) for the control of complex flows (unsteady, turbulent, ...).

In order to tackle such research and development task, it is required to use instead a simple model to predict the momentum (and heat) source that can be effortlessly implemented into commercial solvers to compute the localized addition of momentum (and heat) to the flow at the actuator vicinity. Ideally, a body force model offering a faithful prediction of a single RF-DBD actuator performances depending on its design specifications (e.g. dielectric thickness, electrode separation) and operation settings (e.g. applied voltage, driving frequency). Various models have been derived from theoretical or phenomenological considerations and assessed with more or less success.[9,11] The model of Shyy *et al.*,[12] probably the most employed, has proven to be satisfactory but yet formally complicated and requiring the knowledge of some characteristics specific to the actual DBD discharge such as the charge density or the discharge spatial extent, inconvenient for straight implementation into commercial CFD solvers. Sing*et al.*[13] have derived a simple analytical expression of the EHD force distribution that presents the expected simplicity but however fails in predicting the EHD force magnitude. Later, Soloviev[14] proposed a simple formula of the integral value of the body force that also present the expected simplicity but however has to be distributed adequately prior to any inclusion into CFD computations. On the basis these two last works, the current study intends to establish an upgraded expression for the EHD body force distribution produced by a generic RF-DBD plasma actuator depending on its design and operating settings, presented in Section 2. The validity of the resulting expression is assessed in the case of simple configuration of involving multiple actuator and computed with Fluent presented in Section 3. Flowfield computations obtained in case of in-series actuators configuration and in the case of flipped actuators configuration are discussed respectively in Sections 4 and 5, and compared with empirical data taken from the literature. The study is concluded in Section 6 by exposing the prospective investigations.

2. EHD body force distribution for a single RF-DBD plasma actuator

As a matter of fact, the performances of a single RF-DBD plasma actuator are tightly dependent on the design specifications (dielectric thickness and properties, electrodes length and shape, etc) and on the powering settings (voltage, frequency). In the present study we consider models enabling a fair estimation of the EHD force depending on a minimum set of actuator specifications to ease implementation as body force source term into commercial flow solvers with aim of assessing multi-actuators system concepts.

2.1 EHD force magnitude

We consider first the model established by Soloviev[14] to estimate the integral force produced per unit length of the exposed electrode. Starting from theoretical and numerical modeling of a single micro-discharge, Soloviev has derived a simple formulae to calculate the averaged thrust generated by a single actuator specified by its thickness d and operating at voltage V (peak-to-peak) and at driving frequency f. The thrust produced through ion-neutral momentum transfer is estimated addressing the electronic discharge, the self-consistent electric-field, the probability of negative ion formation and their residence time within the electric field. The resulting relation between the generated force and the actuator specifications is expressed as :

$$T_{Sol}(V,f,d) \approx 2.4\times10^{-10}\alpha_l^4 \cdot \frac{f}{d}\left(\frac{9V}{4\Delta V_c}\right)^4\left(1-\frac{7\Delta V_c}{6V}\right)^4\left(1-exp\left(-\frac{1}{4f\Delta\tau_q}\right)\right) \quad \mathrm{N\cdot m^{-1}} \tag{1}$$

where ΔV_c is the normal falldown of cathode voltage set to 600 V; $\Delta\tau_q$ refers to the negative ions residence time, inferred from their drift time along the dielectric surface and set to $100\mu s$; α_l is a fitting parameter set to 1.0. The calculated thrust was found to be in fair agreement with thrust measurements reported in[15] for a single DBD plasma actuator. Although predicted thrust can values differ from several dozen of percent from empirical data, the overall qualitative agreement as well as its simplicity make the model relevant and convenient for thrust estimation with acceptable accuracy over a large range of operating conditions.

2.2 EHD force distribution

In order to apply this model as body force source term in CFD computations, it shall be appropriately distributed. For such task we consider the model proposed by Sing *et al.*[13] obtained from detailed computations of the DBD discharge dynamics driven by an alternating electric field. Using a two-dimensional finite element based formulation of the plasma coupled with Poisson's equation, they solved for continuity equations governing densities of electrons, ions,

DOI: 10.13009/EUCASS2017-122

Table 1: Overall parameters of the upgraded EHD force model

α_l	ΔV_c (V)	$\Delta\tau_q$	F_{x0}	F_{y0}	β_x	β_y	$\|\vec{F}_{fit}\|$
1	600	10^{-4}	2.6	2.0	$8{\cdot}10^5$	10^7	$7.5359{\cdot}10^{-6}$

and neutral species of nitrogen and oxygen to document on the spatial and temporal distribution of densities and electric potential. From the computed time-averaged body force distribution, they have approximated an analytical expression which depends explicitly on the applied voltage V:

$$\vec{F}_{Sin}(V,x,y;x_0,y_0) = F_{x_0}\cdot V^4 \exp\left[-\left(\frac{x-x_0-(y-y_0)}{y}\right)^2 - \beta_x(y-y_0)^2\right]\hat{\imath} + F_{y_0}\cdot V^4 \exp\left[-\left(\frac{x-x_0}{y}\right)^2 - \beta_y(y-y_0)^2\right]\hat{\jmath} \quad (2)$$

where x_0 is the midpoint between the electrodes and y_0 is at the dielectric surface. F_{x_0}, F_{y_0} designate the average thrust parameters, and β_x, β_y are function of the dielectric material and actuator design. The values of those parameters were tunned to match the distribution of velocity induced by the EHD force in their computations and are specified in Table 1. Since they have obtained very small increase in the induced velocity with the applied frequency and design variation, the resulting functional relationship is merely dependent on the applied voltage to the power four. Computations of the actuated flow using this expression leads to unrealistic values of the induced velocity (also said by the authors), beyond 100 ms^{-1} for voltage above 10 kV. It stems essentially to the fact that the magnitude of the approximated force increases with the voltage to the power four which is clearly a too crude simplification. With this respect, the model is not applicable for thrust prediction but we can reasonably assume that the distribution, because fitted on exact computations, provide a reliable basis to distribute appropriately a reliable total thrust value.

2.3 Upgraded EHD force model

To some extent, each of the two models provide a partial but complementary information on the EHD force generated by a generic actuator: either its global value (without documenting its spatial distribution) or its spatial distribution (with unreliable determination of the thrust magnitude). On this basis, we approximate the distributed EHD body force, in the case of a single generic actuator, multiplying the total thrust term of Soloviev by the distribution of Sing *et al.* normalized to one:

$$\vec{F}_{EHD}(V,f,d,x,y;x_0,y_0) = T_{Sol}(V,f,d)\times\frac{\vec{F}_{Sin}(V,x,y;x_0,y_0)}{\|\vec{F}_{Sin}(V,x,y;x_0,y_0)\|} \quad (3)$$

Expressing the distribution $\vec{F}_{Sin}(V,x,y;x_0,y_0)$ in the following form: $\vec{F}_{Sin}(V,x,y;x_0,y_0) = V^4\cdot\vec{F}_{fit}(x,y;x_0,y_0)$, the approximate body force distribution generated by a single actuator of thickness d operated at voltage V and RF frequency f, and which center is located at x_0, y_0, is then expressed as:

$$\vec{F}_{EHD}(V,f,d,x,y;x_0,y_0) = T_{Sol}(V,f,d)\times\frac{1}{\|\vec{F}_{fit}(x,y;x_0,y_0)\|}\cdot\left\{\exp\left[-\left(\frac{x-x_0-(y-y_0)}{y}\right)^2 - \beta_x(y-y_0)^2\right]\hat{\imath} + \exp\left[-\left(\frac{x-x_0}{y}\right)^2 - \beta_y(y-y_0)^2\right]\hat{\jmath}\right\} \quad (4)$$

With $\|\vec{F}_{fit}(x,y;x_0,y_0)\|$ referring to the magnitude of the distribution $\vec{F}_{Sin}$ which independent on the voltage and determined by means of the double numerical integration. The resulting expression is explicitly depending on the design and operating settings of the actuator as expected, namely the dielectric thickness, the applied voltage and frequency. But also, the expression includes implicit dependencies to the design through parameters for which constant values are adopted and gathered in Table 1.

DOI: 10.13009/EUCASS2017-122

3. Multiple actuators configurations and flow computation

3.1 Multiple-actuators configurations

In order to evaluate the performance of the EHD body force model reported in Eq. 4 for the case of multiple-actuators configuration, we consider two distinct arrangements combining several actuators.

The first configuration consists of multiple actuators arranged in-series on a flat wall surface: in-series actuators configuration. With such arrangement, the momentum transfered by every single actuator is cumulated streamwise. The goal of in-series actuators concept is twofold: an enhancement of the electric wind velocity and a thickening of the actuated layer at the surface vicinity specifically to target large-scale applications, as shown in Fig. 1 in the case of two actuators. Starting from the EHD body force distribution model for a single actuator (Eq. 4), the resulting EHD body force in the case of in-series actuators arrangement can be formulated as:

$$\vec{F}_{inseries} = \sum_{i=1,N_{act}} \vec{F}_{EHD}(V, f, d, x, y; x_i, y_i) \tag{5}$$

where the sum is done over N_{act} actuators displayed in-series, each located on the surface at x_i and y_i.

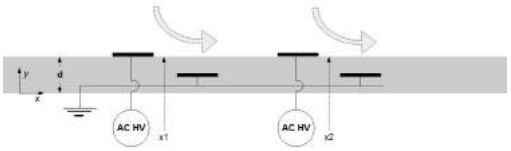

Figure 1: Multi-actuators system: in-series actuators configuration.

The second configuration consists of 2 actuators displayed in mirror, by flipping one actuator: flipped actuators configuration. In such manner, two tangential jets oriented one against the other one are generated and as combination they produce a vertical jet as shown in Figure 2. In this situation, the EHD force can be formulated as:

$$\vec{F}_{flipped} = \vec{F}_{EHD}(V, f, d, x, y; x_{left}, y_{left}) - \vec{F}_{EHD}(V, f, d, -x, y; x_{right}, y_{right}) \tag{6}$$

where $x_{left/right}$ and $y_{left/right}$ refer to the position of left/right actuator of the arrangement, with a separation or gap defined by $x_{right} - x_{left}$ (and $y_{left} = y_{right}$).

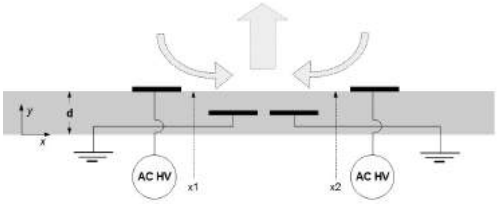

Figure 2: Multi-actuators system: flipped actuators configuration.

3.2 Flow computation

The actuated flow obtained with the selected configurations is estimated by means of commercial solver FLUENT assuming a non-compressible still air of density constant 1.225 kg.m^{-3}. The flow-field is obtained by solving for the steady Reynolds-Averaged Navier-Stokes (RANS) equations with the Spalart-Allmaras equation turbulence model, expressed in terms of the eddy viscosity, well-suited for low-Reynold regime. In the present study, the actuator effect has been modeled as a source term to the momentum conservation equation expressed as:

DOI: 10.13009/EUCASS2017-122

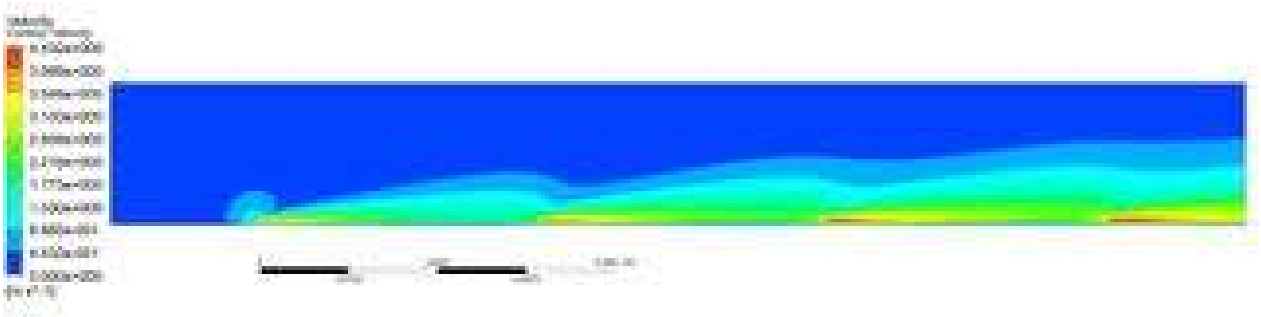

Figure 3: Velocity contour map in the case of 4 in-series actuators configuration, 1kHz, 3mm dielectric thickness.

$$\frac{\partial}{\partial t}(\rho\vec{v}) + \nabla \cdot (\rho\vec{v}\vec{v}) = \nabla p + \nabla \cdot \overline{\overline{\tau'}} + \rho\vec{F_{EHD}} \tag{7}$$

where ρ is the air density, v the speed, p the pressure and τ' the viscous stress tensor. The model is implemented on the basis of the User Defined Function (UDF) tool to the whole domain of computation. The equations are spatially discretized in the framework of the cell-centered finite-volume method, and the second-order upwind scheme is used to discretized the momentum equations and the viscous terms.

The in-series actuators configuration is addressed in a domain of 1.5×16 cm with the first actuator placed 2 cm from the left side. The mesh is generated with 60000 elements, with a bias factor of 7.5 of vertical resolution towards the lower wall, for a better definition of the forces at the actuators vicinity. The flipped actuators configuration is addressed in a domain of 5×8 cm, with the arrangement centered in the domain. The mesh features an even configuration of 256000 elements. In the case of jet vectoring, the mesh was biased to the bottom of the control volume to define better the resolution with a bias factor set to 7.5. The boundary conditions of the domain were set to pressure-outlet for left, right and upper boundaries. The lower limit of the domain was set to solid wall conditions wall applying the no-slip condition.

The convergence histories of residuals and forces have been assessed adopting a convergence criterion for the dimensionless residual less than a limit value set to 10^{-5} for mass conservation equation and to 10^{-9} for the x-velocity, y-velocity and turbulent kinematic viscosity. The time needed for each iteration is around one second with an ordinary laptop computer (~2.4 GHz processor) and the computations have converged after around 10^4 and $\times 10^5$ iterations, respectively for the in-series and flipped actuators configuration.

4. In-series actuators

We apply the EHD force model 4 to simulate the flow actuated by means of in-series actuators configuration as described in Section 3.1. We replicate the experiments of Moreau *et al.*[16] performed in ambient air with a system made of four actuators arranged in-series and placed sufficiently close to enhance the accumulation effect along successive actuators. However because of the proximity between the actuators, the successive exposed electrodes have been alternatively set to high-voltage and to ground, in order to cancel the mutual interaction between two successive actuators (caused by back-discharge from each air-exposed electrode toward the grounded electrode of the previous single DBD). Besides, in their setup, the exposed electrodes are not flat but instead made of thin wires of 25 μm diameter in order to enhance the electric wind produced by each single actuator. Also, claiming for performance enhancement, they used a dielectric layer combining a first layer of PMMA of 3 mm thickness with a second layer of Kapton of 75 μm thickness. Velocity measurements have been conducted with a Pitot tube to document horizontal velocity profiles measured at 0.6 mm above the wall, with actuators operated at 16, 20 and 24 kV at even driving frequency of 1 kHz.

The substantial thickening of the actuated boundary layer following on the momentum accumulation is clearly appreciable with the evolution of the vertical velocity profiles v_x along y evinced in Fig. 4 for each actuators location. The thickening of the actuated boundary layer is considerably increased with the voltage elevation from 16 to 20 kV (meaning the generated the thrust augmentation). At 16 kV, from the first to the last actuator the increase of the maximum is from 0.8 to 1.2 m/s (about 30% increase), while at 20 kV the velocity passes from 1.3 to above 2 m/s (about 40% increase), indicating that the accumulation effect is more pronounced for higher total thrust generated by each actuators.

DOI: 10.13009/EUCASS2017-122

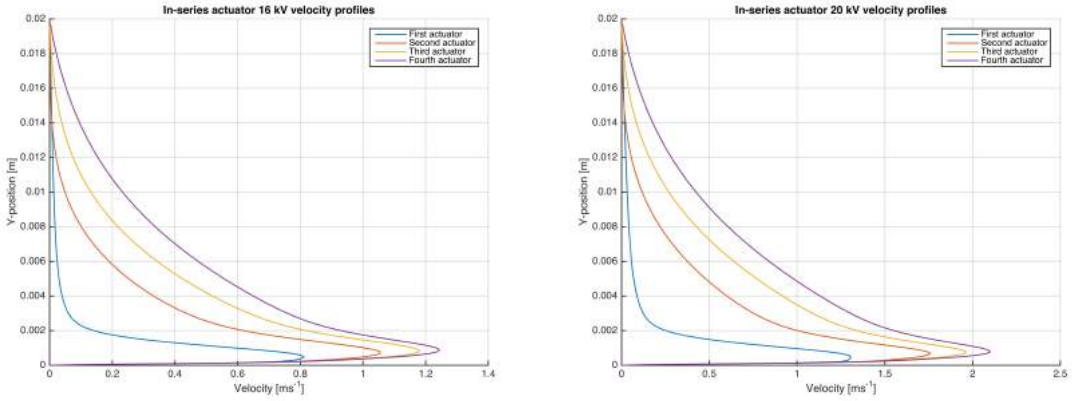

Figure 4: Velocity magnitude profiles along y direction, at each actuator location. At left: 16 kV. At right: 20 kV

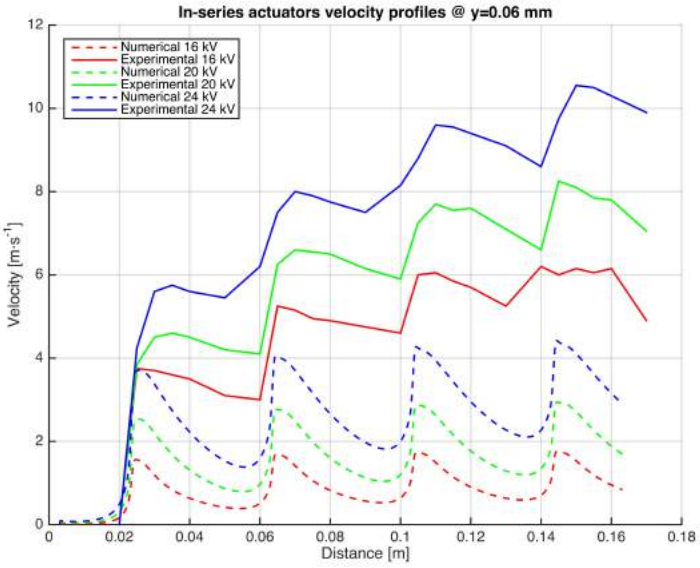

Figure 5: In-series actuators for 1 kHz, 3 mm dielectric thickness. Comparisons between Pitot probe measurements[16] (continuous lines) and computed data (dashed lines).

Comparisons between measurements and computed velocity profiles are reported in Fig. 5. Although the momentum accumulation and profile thickening features are clearly analogous, they differ significantly up to 3 times. It should be reminded that the Soloviev model predicts the actual thrust of a generic actuator with an accuracy of about 50 %. Also the possible sources of discrepancies between our computations and the measurements can come from the particularities of the experimental arrangement. Since the model we use to replicate the actuated flow field take into account only few parameters and is insensitive to deviation from a generic actuator architecture. Indeed the experimental arrangement is based on non-flat electrodes that have demonstrated to have substantial enhancement. This particularity is not addressed in the current modeling approach and substantiate the fact that experimental velocity are systematically higher than those predicted. Also, the experimental arrangement uses a dielectric layer composed of 2 distinct materials. However, the dielectric material property has a marginal influence on the performance actuator in a first order of approximation following the analysis of Sing *et al.*[13] and Soloviev.[14] Therefore, although mixing of dielectrics is present, it is reasonable to consider that this aspect of the design will have a little influence on the replication.

In order to investigate whether the model can yield better agreement for higher thrust value, the actuated flow has been computed assigning a value of 0.15 N/m produced per actuators. The computed velocity profile is compared in Fig.6 to the measurements obtained at 24 kV. An acceptable agreement for the first overshoot is achieved but the rest of the experimental profile follows a more pronounced ascending slope. This could be due to the fact that the

DOI: 10.13009/EUCASS2017-122

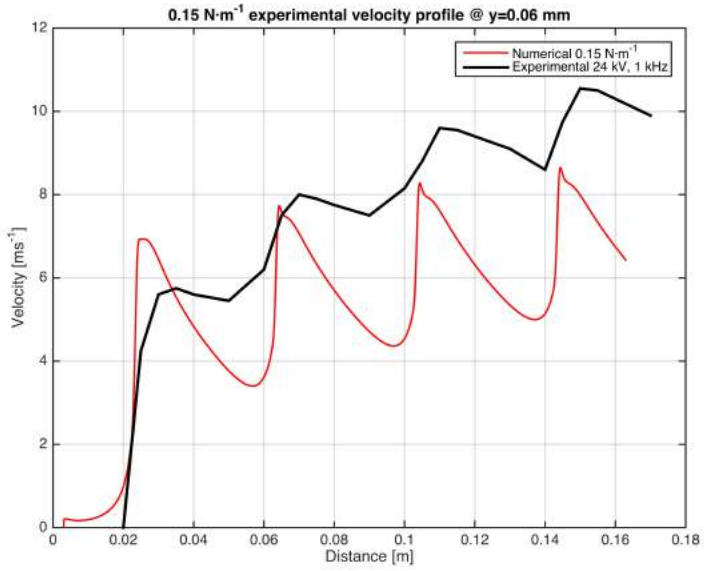

Figure 6: Comparisons between Pitot probe measurements[16] and computed data imposing an even thrust value to each actuator of 0.15 N/m.

experimental actuator produce a thrust along the x direction in a much more elongated fashion than the modeled actuators, then maintaining higher velocities along x direction. The cumulative effect therefore is higher, having a stronger trend streamwise. Hence, for better agreement not only the total thrust but also the structure of the steady body force distribution has to be revisited, especially in the case of 3D shape exposed electrodes. Despite its insufficiencies, the model predicts *in fine* fairly the accumulation of momentum and boundary layer thickening phenomena, that makes it a valuable approach for the assessment of more elaborated configuration within CFD computations.

5. Flipped actuators

5.1 Normal jet

We apply the EHD force model to simulate the flipped-actuators configuration as described in Section 3 to produce a synthetic jet normal to the wall. In a first step, we address the effect of the separation between both actuators involved in the arrangement. A series of computations have been performed for a separation of 0 and 3 mm between actuators, with a fixed dielectric layer thickness set to 1 mm. Each actuator is powered at even driving frequency set to 6 kHz and with applied voltage of 10, 12, 14 and 16 kV corresponding to integrated thrust values of 0.007, 0.015, 0.030 and 0.052 N/m.

The typical resulting flow field in Fig. 7 depicts three distinct regions. At the center there is the symmetric jet characterized by an elevated velocity in the main vertical and oriented to the top. On either side, the wing-like region corresponding to the air transported slowly toward the actuator. And in between, an intermediate region of interaction resulting in recirculation region.

The profiles of the y-wise velocity component v_y, are reported in Fig. 8 at the plane of symmetry of the configuration. The maximum of the vertical jet velocity is achieved at height varying weakly with the conditions and ranges from 5 to 7 mm. The achieved velocity increases with the applied voltage from about 1 to 3.5 m/s. Besides, the separation between actuators has a non negligible effect on the profiles which peaks at higher velocity for gap of 3 mm.

The profiles of x-wise and y-wise components of the velocity, namely v_x and v_y are reported in Fig. 9 at the height of maximum jet velocity. In the wing region, close to the wall, the air seems to be dragged toward the actuators undergoing steady acceleration and achieving a maximum velocity $||v_x||$ peaking at about 0.5 m/s at the frontier with the so-called intermediate region, before dropping in the jet core. In the intermediate region, the flow undergoes a sudden aspiration downward, evidenced by the velocity $||v_y||$ peaking at 0.5 m/s at the same location of $||v_x||$ maximum. Then, the air is "expelled" by each actuator in opposite directions resulting in the formation of a jet normal to the wall. At this vertical location the effect of the gap appears to be more significant on the aspiration process than on the resulting normal jet velocity.

DOI: 10.13009/EUCASS2017-122

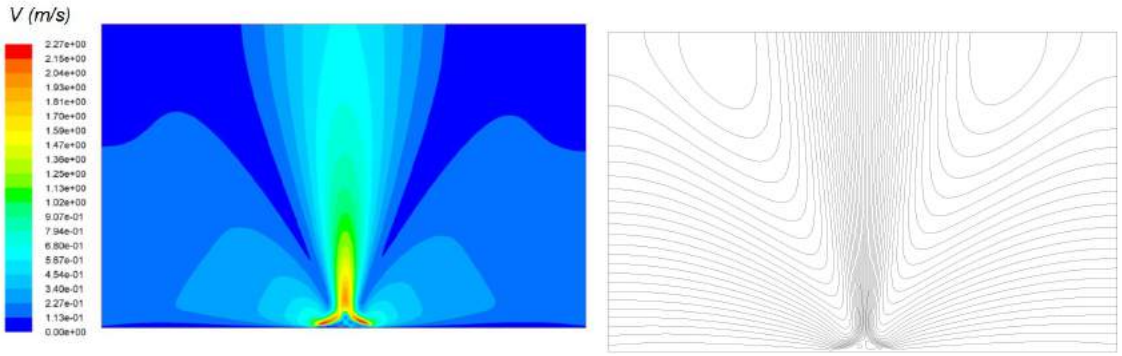

Figure 7: Flipped actuators configuration for 12 kV, 0 mm gap, 6 kHz. At left: velocity contour map. At right: streamlines.

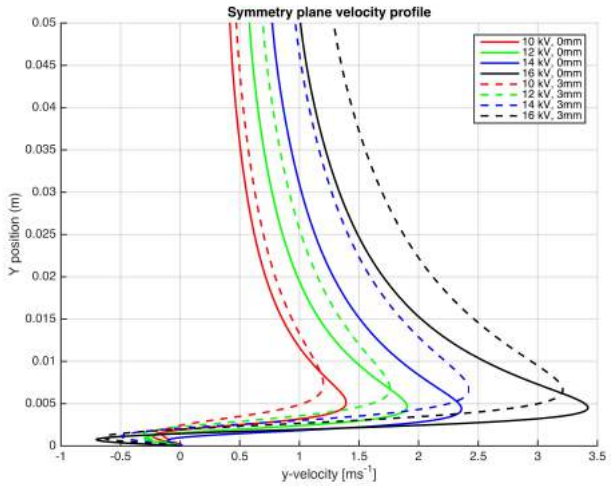

Figure 8: y-wise velocity component at symmetry plane of flipped actuator configuration.

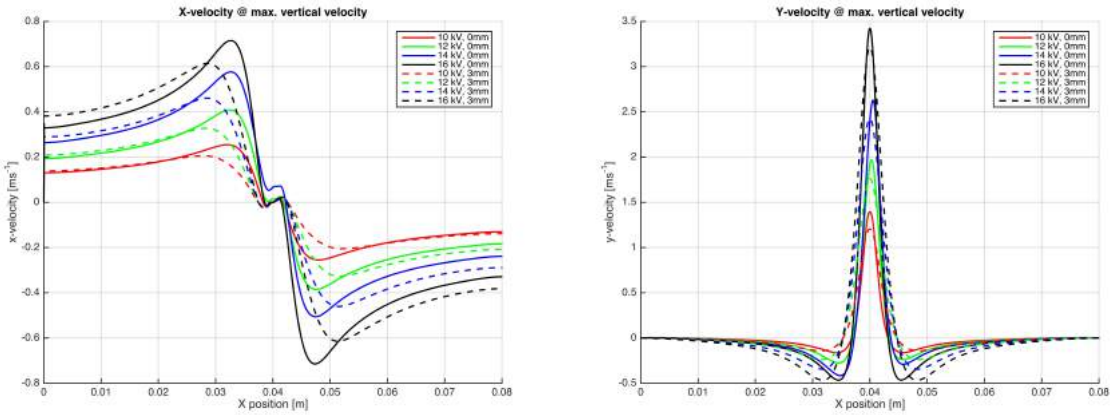

Figure 9: v_x and v_y profiles at $y \sim 0.6$ cm.

DOI: 10.13009/EUCASS2017-122

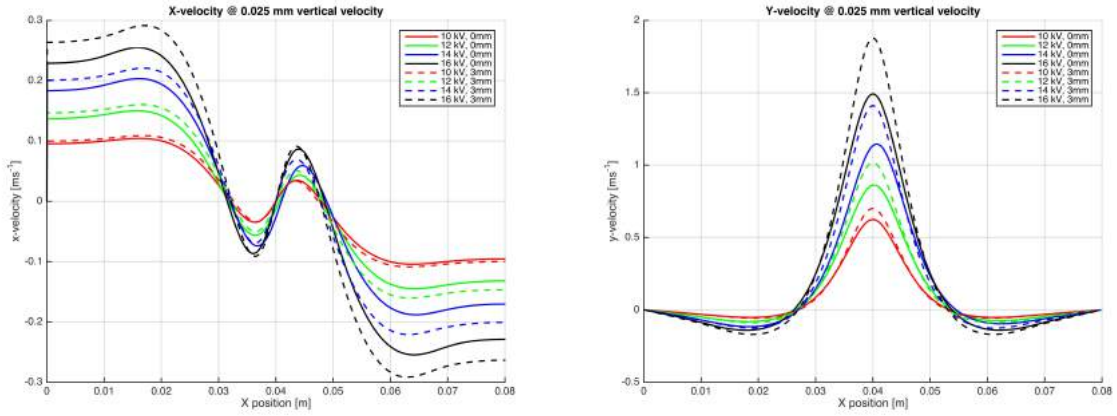

Figure 10: v_x and v_y profiles at $y = 2.5$ cm.

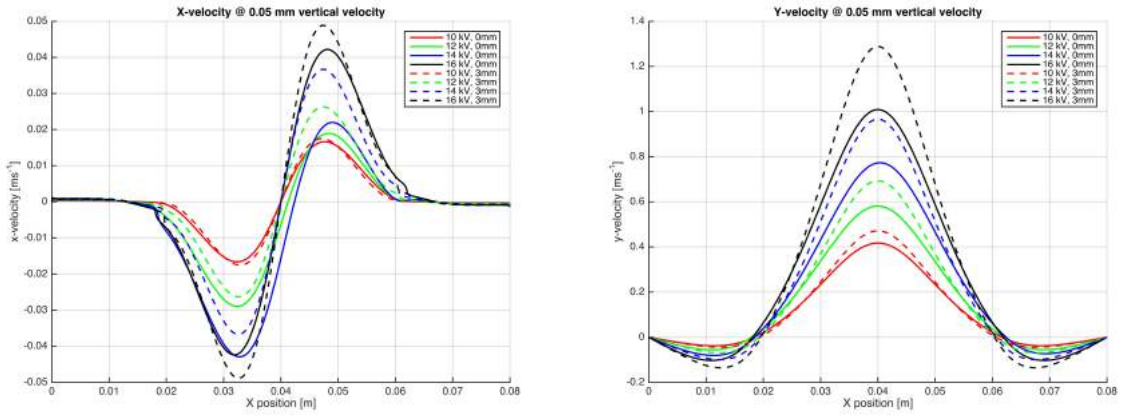

Figure 11: v_x and v_y profiles at $y = 5$ cm.

The v_x and v_y profiles at $y = 2.5$ cm, reported in Fig.10, exhibit the analogous features. In the wing region, the air is dragged toward the actuators and reaches a maximum velocity $||v_x||$ peaking at about 0.3 m/s at 2 cm from the centerline, where the flow also undergoes the strongest aspiration downward with $||v_y||$ peaking at 0.1 m/s. In the core jet, the flow is mainly transported upward, but experiences also slight radial diffusion outwards the jet.

The v_x and v_y profiles at $y = 5$ cm reported in Fig.11 show that the air x-wise dragging from the wing region has faded, while there is still a transport toward the wall with v_y peaking at 0.1 m/s at about 3 cm from the jet centerline. Besides, if the core jet dynamics is dominated by upward transport, the flow experiences also a slight radial diffusion outwards the jet.

A significant outcome is that the characteristic of the resulting normal jet are affected by the separation imposed between the actuators "blowing" in opposite directions. For instance, looking at the velocity achieved downstream in the jet plume at $y = 5$ cm, in the case of a gap of 3 mm, v_y is higher of almost 20% than in the case without separation. In the wake on these results, the adopted model can find valuable application in finding the optimum separation between actuator to enhance performances of resulting the normal jet.

5.2 Vectorized jet

In a second step we address the synthetic jet produced by means of flipped actuators configuration but when each actuator generates different thrust. With such asymmetric thrust production, the combination of the two opposite jets is no more a normal jet but results in a jet deflected by an angle that depends on the difference between thrust provided by each actuators. In practice, such jet vectoring is obtained changing the frequency or the voltage of one actuator with respect to the other one. We replicate here the experiments reported by Bolitho *et al.*[17] for a flipped-actuator configuration. They used linear flat copper electrodes arranged with dielectric layer made of Teflon of 1/8 inch

DOI: 10.13009/EUCASS2017-122

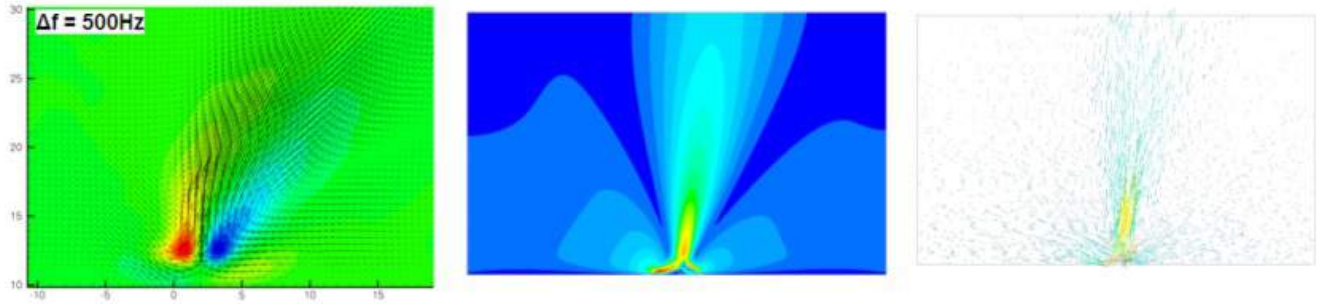

Figure 12: At left: PIV measurements.[17] At the center: Computed velocity contour map. At right: Computed velocity vector field. Computation performed with $T_{left}/T_{right} = 0.82$.

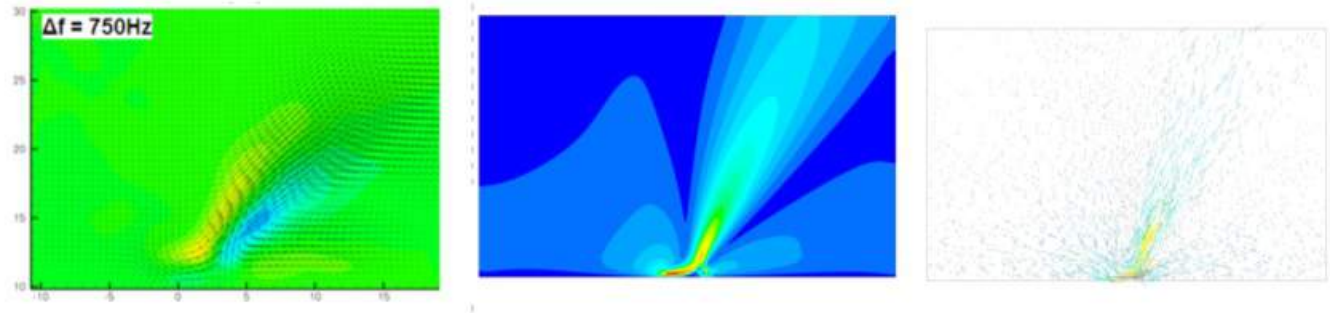

Figure 13: At left: PIV measurements.[17] At the center: Computed velocity contour map. At right: Computed velocity vector field. Computation performed with $T_{left}/T_{right} = 0.56$.

thickness. In particular, the setup consists of two exposed electrodes on either side of a single embedded electrode, meaning that only one grounded electrode is shared by two active electrodes. With this respect, we computed the flipped actuator configuration with no separation. The exposed electrodes are powered with a square waveform voltage with driving frequencies in the range 8-9 kHz. By lowering the driving frequency applied to the right actuator of 500, 750, 1000 Hz, they have obtained a deflected jet which has been characterized by means of Particle Image Velocimetry (PIV) measurement technique.

Since the applied voltage was not reported neither the exact frequency, no quantitative comparisons can be performed. Nevertheless qualitative analysis can be proposed instead. We have computed such vectorized jet for several cases with asymmetric thrust and we have retained those with deflection close to the experimental case. The comparisons between experimental data[17] and computed flow-field are gathered Fig. 12 13 14, respectively in the cases of weak, intermediate and strong deflection, obtained for different ratio between the total thrust generated by the left actuator T_{left} to the right actuator T_{left}. For each situation the qualitative features are well reproduced. In the case of weak deflection the jet keeps its straight rectilinear shape while undergoing the inclination following on the right

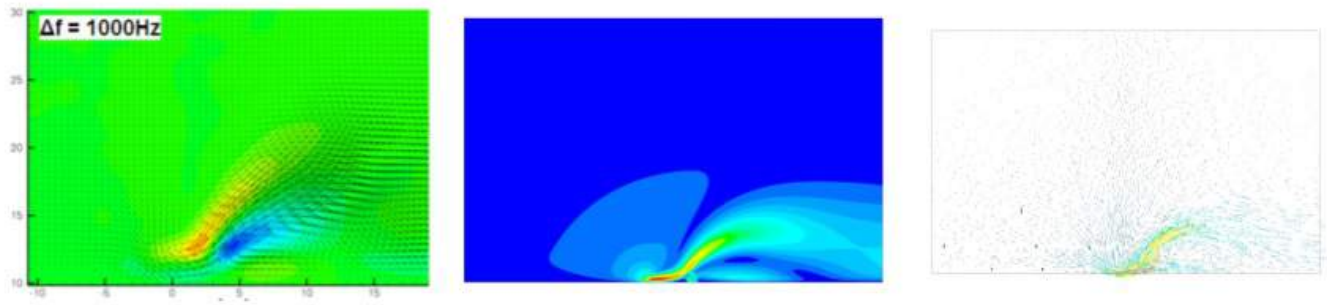

Figure 14: At left: PIV measurements.[17] At the center: Computed velocity contour map. At right: Computed velocity vector field. Computation performed with $T_{left}/T_{right} = 0.45$.

DOI: 10.13009/EUCASS2017-122

actuator thrust diminishing (because of the driving frequency decrease). In the case of strong deflection, the jet is bended following on the interaction with a recirculation structure established between the solid wall an the jet, clearly observed with experimental and computed data.

6. Concluding remarks

The present study was intended to propose an upgraded EHD force expression starting from previously reported simple models. Such simplified description of the EHD force distribution is of great importance to support the evaluation of any flow control system that includes multiple RF-DBD plasma actuators. For instance large scale actuator arrangement combining numerous actuators and displayed on complex geometries. In that perspective, the upgraded model has been elaborated and tested by means of ordinary commercial solver in the cases of a modest configuration of multi-actuators. The in-series actuators and the flipped actuator have been addressed on the basis of documented experiments. The comparisons between experimental data and computed properties of the actuated flow-field have evidenced for the adequate performance of the model, which can ease the development and optimization of large-scale DBD actuator systems. Nevertheless the model requires still improvement to achieve more accurate values.

7. Acknowledgments

This project has received funding from the Universidad Carlos III de Madrid, the European Union's Seventh Framework Programme for research, technological development and demonstration under grant agreement №600371, el Ministerio de EconomÃa, Industria y Competitividad (COFUND2013-40258), el Ministerio de Educación, cultura y Deporte (CEI-15-17) and Banco Santander.

References

[1] J. R. Roth, D. M. Sherman, and S. P. Wilkinson, "Electrohydrodynamic flow control with a glow-discharge surface plasma," *AIAA journal*, vol. 38, no. 7, pp. 1166–1172, 2000.

[2] T. Corke, E. Jumper, M. Post, D. Orlov, and T. McLaughlin, "Application of weakly-ionized plasmas as wing flow-control devices," in *40th AIAA Aerospace Sciences Meeting & Exhibit*, p. 350, 2002.

[3] M. L. Post and T. C. Corke, "Separation control on high angle of attack airfoil using plasma actuators," *AIAA journal*, vol. 42, no. 11, pp. 2177–2184, 2004.

[4] F. O. Thomas, A. Kozlov, and T. C. Corke, "Plasma actuators for cylinder flow control and noise reduction," *AIAA journal*, vol. 46, no. 8, pp. 1921–1931, 2008.

[5] D. M. Orlov, G. I. Font, and D. Edelstein, "Characterization of discharge modes of plasma actuators," *AIAA journal*, vol. 46, no. 12, pp. 3142–3148, 2008.

[6] E. Moreau, "Airflow control by non-thermal plasma actuators," *Journal of Physics D: Applied Physics*, vol. 40, no. 3, p. 605, 2007.

[7] T. C. Corke, C. L. Enloe, and S. P. Wilkinson, "Dielectric barrier discharge plasma actuators for flow control," *Annual review of fluid mechanics*, vol. 42, pp. 505–529, 2010.

[8] C. Enloe, T. E. McLaughlin, R. D. Van Dyken, K. Kachner, E. J. Jumper, and T. C. Corke, "Mechanisms and responses of a single dielectric barrier plasma actuator: plasma morphology," *AIAA journal*, vol. 42, no. 3, pp. 589–594, 2004.

[9] J. R. Roth, "Aerodynamic flow acceleration using paraelectric and peristaltic electrohydrodynamic effects of a one atmosphere uniform glow discharge plasma," *Physics of plasmas*, vol. 10, no. 5, pp. 2117–2126, 2003.

[10] A. V. Likhanskii, M. N. Shneider, S. O. Macheret, and R. B. Miles, "Modeling of dielectric barrier discharge plasma actuator in air," *Journal of Applied Physics*, vol. 103, no. 5, p. 053305, 2008.

[11] K. Hall, E. Jumper, T. Corke, and T. McLaughlin, "Potential flow model of a plasma actuator as a lift enhancement device," in *43rd AIAA Aerospace Sciences Meeting and Exhibit*, p. 783, 2005.

[12] W. Shyy, B. Jayaraman, and A. Andersson, "Modeling of glow discharge-induced fluid dynamics," *Journal of applied physics*, vol. 92, no. 11, pp. 6434–6443, 2002.

DOI: 10.13009/EUCASS2017-122

[13] K. P. Singh and S. Roy, "Force approximation for a plasma actuator operating in atmospheric air," *Journal of Applied Physics*, vol. 103, no. 1, p. 013305, 2008.

[14] V. Soloviev, "Analytical estimation of the thrust generated by a surface dielectric barrier discharge," *Journal of Physics D: Applied Physics*, vol. 45, no. 2, p. 025205, 2011.

[15] F. O. Thomas, T. C. Corke, M. Iqbal, A. Kozlov, and D. Schatzman, "Optimization of dielectric barrier discharge plasma actuators for active aerodynamic flow control," *AIAA journal*, vol. 47, no. 9, pp. 2169–2178, 2009.

[16] E. Moreau, A. Debien, N. Bénard, T. Jukes, R. Whalley, K. Choi, A. Berendt, J. Podlinski, and J. Mizeraczyk, "Surface dielectric barrier discharge plasma actuators," *ERCOFTAC Bull*, vol. 94, no. 5, 2013.

[17] M. Bolitho and J. Jacob, "Thrust vectoring flow control using plasma synthetic jet actuators," in *46th AIAA Aerospace Sciences Meeting and Exhibit*, p. 1368, 2008.